Measurements and modelling of solid phase lithium sputtering

2002 Nucl. Fusion 42 202

(http://iopscience.iop.org/0029-5515/42/2/312)

INSTITUTE OF PHYSICS PUBLISHING and INTERNATIONAL ATOMIC ENERGY AGENCY NUCLEAR FUSION

Nucl. Fusion **42** (2002) 202–210 PII: S0029-5515(02)33447-1

Measurements and modelling of solid phase lithium sputtering

J.P. Allain, D.N. Ruzic

University of Illinois, Urbana, Illinois, United States of America

E-mail: jp@starfire.ne.uiuc.edu

Received 25 April 2000, accepted for publication 17 July 2001
Published 15 February 2002
Online at stacks.iop.org/NF/42/202

Abstract

The absolute sputtering yields of D^+, He^+ and Li^+ on deuterium saturated solid lithium have been measured and modelled at 45° incidence in the energy range 100–1000 eV. The Ion–surface InterAction Experiment (IIAX) was used to measure the absolute sputtering yield of lithium in the solid phase from bombardment with a Colutron ion source. The lithium sample was treated with a deuterium plasma from a hollow cathode source. Measurements also include bombardment of non-deuterium-saturated lithium surfaces. The results lead to the conclusion that the chemical state of the deuterium treated lithium surface plays a major role in the decrease of the lithium sputtering yield. Specifically, preferential sputtering of implanted deuterium atoms over lithium atoms in deuterium treated samples results in a decrease of at least 60% of the lithium sputtering yield, in the case of He^+ bombardment. These results also demonstrate that lithium self-sputtering is well below unity and that the fraction of sputtered species in an ionic state ranges from 55 to 65% for incident particle energies between 100 and 1000 eV. Furthermore, correlation of Monte Carlo VFTRIM-3D simulations and IIAX experimental data demonstrate that the surface composition has a one to one ratio between deuterium and lithium components.

PACS numbers: 52.55.-s, 79.20.Rf

1. Introduction

The choice of materials for the first wall and divertor in fusion reactor experiments is crucial for the performance of thermonuclear fusion plasmas. Extensive research has been done to determine which materials would survive yet not degrade plasma performance in tokamak plasmas [1–3]. Low Z materials have been proposed as an attractive alternative to high Z materials. Of these, the prime candidates are beryllium and graphite. Graphite has been the usual choice for a first wall material due to its low Z characteristic along with its superior thermomechanical properties [4]. Graphite, however, suffers from temperature dependent chemical sputtering and radiation enhanced sublimation reactions, leading to a net increase in its erosion yield [5, 6]. Beryllium has been measured to have fairly low sputtering yields while enhancing plasma performance [7–10]. Beryllium, however, does not possess the attractive thermophysical properties of graphite.

Recently several articles have summarized the role of lithium wall conditioning that led to a dramatic decrease in carbon impurities in TFTR [11, 12]. Thus lithium has become an attractive first wall or divertor material candidate not only due to its low Z and relatively good thermophysical properties, but also due to its ability to absorb impinging species. The ability of lithium to strongly absorb impinging D–T ions may lead to a high temperature/low density or 'low recycling' regime [13]. A low melting point could be a disadvantage, however, it could allow continuous recovery of damaged surfaces exposed to the large heat fluxes in the reactor wall and divertor regions.

Although there are attractive characteristics in using lithium as a plasma facing material, the modelling predictions made by László and Eckstein show relatively high sputtering yields from both deuterium and lithium bombardment [14]. Although higher anticipated sputtering yields would exist in comparison with other materials, the amount of lithium impurities sputtered into the plasma would be tolerable. The experimental determination of how large the lithium sputtering yields from deuterium, helium and lithium bombardments are provides the motivation for the work of this article. In addition, determining the effect of a deuterium treatment of the lithium surface on lithium sputtering is also of interest, as well as determining the fraction of sputtered species in the ionic state. The latter is especially important since sputtered lithium ions will immediately return to the surface due to the magnetic sheath potential configuration at the plasma edge in tokamaks.

The VFTRIM-3D simulation is used along with the experimental results to gain more insight into the physical processes that occur in low energy sputtering events of deuterium treated and non-deuterium-treated solid lithium.

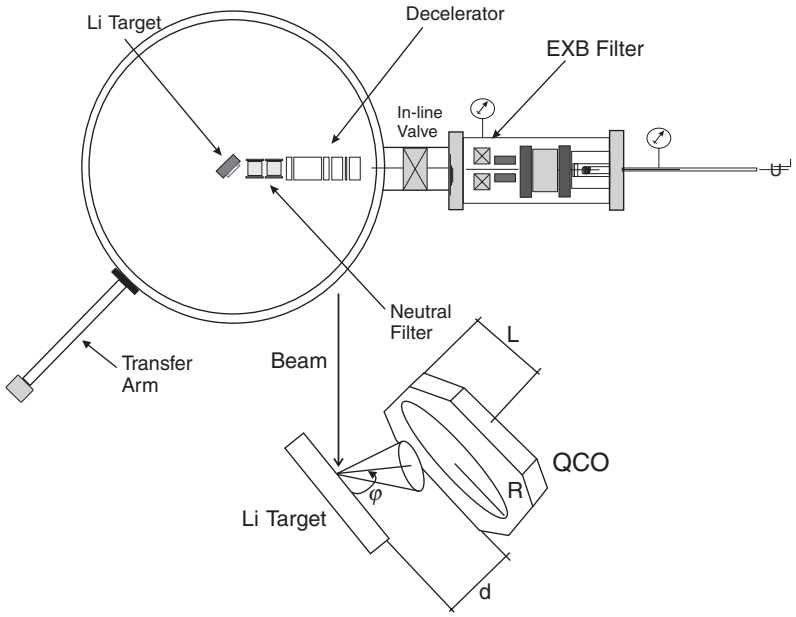

Figure 1. The IIAX experimental device with two differentially pumped chambers. On the right, the ion gun chamber and, on the left, the main chamber where the lithium target sample is located. The inset diagram shows the position of the quartz crystal oscillator (QCO) with respect to the lithium target. The distance between the lithium target and the QCO is d, the angle of ejected flux φ, the radius of the crystal R and the length from the edge of the QCM to the centre of the crystal is designated L.

VFTRIM-3D is a variant of the TRIM code which includes fractal surfaces and a low energy non-binary collision model [7, 15]. To complement simulation work, a semi-empirical analytical model known as the Bohdansky formula based on Sigmund's linear cascade theory is also utilized. The model is coupled to Yamamura's formulation for oblique incidence and a model designed to account for preferential sputtering of embedded species.

2. Experimental design and set-up

The Ion–surface InterAction Experiment (IIAX) is designed to measure the absolute, angular resolved and self-sputtering yields of many particle/target combinations (Fig. 1). A Colutron ion source is used to create and accelerate gaseous or metal ions onto a 100 mm^2 metal target. Gaseous ions are obtained by means of electron impact ionization while lithium metal ions are obtained by thermionic emission from a LiCl powder. The bombarding ions are mass selected through an $\boldsymbol{E} \times \boldsymbol{B}$ filter and decelerated near the target by a five element cylindrical electrostatic lens system. Complete details of the system can be found in earlier papers [7,16]. Deceleration near the target effectively reduces the time of interaction between ions in the beam as they transit the system from source to target location. This is important due to spreading of the beam from space charge effects [17]. Since the beam carries both an ionized and a neutral component, a neutral filter is placed between the decelerator and the target to remove the neutral component of the beam. The target can be rotated in order to provide variation in the angle of incidence. For this experimental campaign an angle of incidence of 45° was used based on the average angle of incidence of a gyrating particle at locations where the magnetic field lines cross the divertor plates at oblique incident angles (see chapter by R. Chodura in Ref. [2]).

A hollow cathode source is used to provide plasma cleaning of the target, leading to the removal of any oxides or other impurities from the surface. A 420 mtorr deuterium plasma irradiates the lithium sample for twenty minutes with an incident flux averaging 2×10^{16} ions/(cm^2 s^{-1}). This method also allows for the treatment of the lithium sample with deuterium, simulating plasma-facing wall conditions within a fusion reactor. This flux level is sufficient to obtain a one to one ratio of deuterium atoms to lithium atoms as measured by H. Sugai [18]. For the incident energy of deuterium ions the incident ion range is 305 Å with a latitude straggle of 140 Å, calculated by TRIM-SP.

The partial pressure of the system is monitored with a quadrupole gas analyser. Typical operating pressures before the beam is switched on are 10^{-6}–10^{-5} Pa. Fluxes of the order of (2–4) $\times$ 10^{13} ions/(cm^2 s) can be achieved with an average beam spot diameter of 1.0 mm. A 0.75 mm thick and 100 mm^2 area lithium target is inserted in the main chamber under a 13.8 kPa argon atmosphere to prevent oxidation of the lithium target.

A dual quartz crystal microbalance (QCM) unit is rotated in front of the target to collect the sputtered flux. Environmental influences on the frequency variation of a QCM have been extensively studied including charging, crystal strain-relaxation effects, adsorption, desorption and chemical reactions [19]. Owing to the dependence of the QCM unit on ambient temperature, a new technique has been applied to compensate for ambient temperature variations over time. This new technique allows not only for the compensation of temperature effects but also for mechanisms such as adsorption/desorption of residual gases such as oxygen, water and nitrogen. This technique has increased the signal to noise ratio by a factor of 25 over previously used techniques [7]. The mechanism works by using a dual QCM unit, which consists of

two gold coated quartz AT cut crystals, in thermal contact, with a fundamental frequency of the order of 6 MHz. One sensor acts as the deposition crystal, the other as a reference crystal. Deposition of the sputtered flux is measured by a decrease in frequency as mass is collected on the deposition crystal. A background trace monitors both crystals for a period of 15–24 h before and after beam irradiation. Although the surfaces of the two crystals are not exactly the same, the difference in frequency is within ± 0.5 Hz or ± 0.25 Å at most. The uncertainty in the measurement of the lithium yield will be discussed in detail in the next section. After the proper dose is obtained the QCM dual unit is rotated away from the target and both crystals are kept running. After reaching equilibrium, the background frequency signal is measured for another 10–15 h. The frequency variation of the deposition crystal is correlated with the mass loss of the sample as shown quantitatively in the next section.

3. Data analysis and calculations

Analysis of the absolute sputtering yield of lithium begins by correlating the frequency variation in the crystal signal with the time period of the ion beam dose. A least squares fit with a weighting of $1/\Delta f^2$ is calculated for the raw frequency difference data between the deposition and reference crystals. The slopes of these fits, in Hz/s, are then used along with the time period of the dose to obtain a loss in frequency Δf, corresponding to the mass gain on the crystal, which is the mass loss from the lithium sample. For the background frequency a similar weighted least squares fit is applied to the QCM difference trace 'weighed' by the respective time interval of frequency variation (increase or decrease). The uncertainty for the decrease in QCM frequency over the respective time intervals ranges from 30 to 40%.

The sputtered lithium flux is assumed to have a skewed distribution with respect to the surface normal due to oblique particle incidence. This is incorporated in the calculation of the fraction of sputtered flux collected by the QCO, denoted as Ω. This fraction accounts for the location of the crystal with respect to the lithium sample by integrating over the azimuthal angle and the radial distance from the emission point to the collection centre. The relevant distances are shown in the inset of Fig. 1. The QCM system is mounted on a manipulator, and thus its spatial and angular positions with respect to the target are known. Although the QCM location is known absolutely, uncertainty as to the actual angular sputtered distribution exists. An estimate is calculated by use of VFTRIM-3D, which leads to an uncertainty of about 40% in the measurement of the lithium sputtering yield.

The other mechanism of importance in the measurement of the lithium sputtering yield is the sticking coefficient of lithium atoms onto the QCM crystal. The standard QCM crystals are covered with a thin gold film. Sputtered lithium atoms from a 700 eV D^+ beam at 45° incidence have an average energy of 20 eV according to the VFTRIM-3D simulation. At this energy, if the QCM crystal was solely covered with gold, only 25% of the sputtered lithium atoms 'stick'. Therefore a thin, 260 μm, carbon film was evaporated on the gold surface ex situ, increasing the sticking coefficient to an average of 84% for the case of a QCM crystal covered with the concentrations measured by X ray photoelectron spectroscopy (XPS) and Auger electron spectroscopy (AES). The addition of this carbon film increased the amount of collected sputtered flux by a factor of 3, consequently improving absolute sputtering yield measurements by maximizing the probability of sputtered lithium sticking to the gold covered QCM crystal. Uncertainty analysis on the value of the lithium sticking coefficient results in a 25% uncertainty. The sticking coefficients used in the analysis of the lithium sputtering yield are tabulated in Table 1.

The mass collected on the crystal is assumed to be that of Li_2O, m_{Li_2O}, and not atomic lithium. The average incident flux of O_2 onto the QCO face, ranges from 4.0×10^{12} to 2.0×10^{13} O_2 molecules/(cm^2 s). Therefore, with the ultimate pressure of the chamber ranging from 8×10^{-6} to 9×10^{-6} Pa, oxides will adsorb on the carbon surface of the QCM crystal and form bonds with the deposited lithium. On the surface, lithium will either diffuse into the hexagonal close packed (HCP) carbon lattice forming bonds with oxygen at the basal planes [18,20,21] or form oxides at the surface. Therefore, the mass obtained is that of lithium oxide, 29.88 g/mol, and not pure lithium, 6.9 g/mol. This observation has been verified with XPS and AES measurements of the QCO surface after lithium sputtering measurements were completed. The results conclude that 46% carbon, 36% lithium and 18% oxygen are found on the surface of the QCM crystal. These measurements confirm lithium intercalation into graphite basal planes, since the top layer is not 100% Li_2O, similar to AES results found by Sugai [18].

Oxidation of the lithium target is important. However, if oxygen also played a significant role in the effective decrease of the lithium sputtering yield, this would have been measured in real time by the QCO signal. A decrease of the lithium sputtering yield over the time of dose would have been manifested in a decrease in the slope of the frequency versus time trace. This has not been found; therefore the likelihood that oxidation plays a role in the decrease of the lithium sputtering yield is small. However, the chemical state of the target before ion beam irradiation may play a significant role in the decrease of the lithium sputtering yield. In the solid phase, bonding between lithium and deuterium atoms is less likely than for deuterium atoms implanted at interstitial sites in the lithium lattice. This phenomenon has been investigated in great detail by Sugai [18] and co-workers. Thus Li–D binding is less likely to be a factor in the effective decrease of lithium sputtering. Rather, preferential sputtering of embedded deuterium atoms at interstitial sites in body centred cubic (BCC) lithium leads to a significant decrease of lithium sputtering.

In order to resolve how significantly this accumulation of oxygen on the surface influences the lithium sputtering yield, data for the non-deuterium-treated lithium case with helium bombardment were collected for incident oxygen fluxes of 2×10^{13} and 3.6×10^{10} O_2 cm^{-2} s^{-1}. If oxygen played a role in the lithium sputtering yield decrease a significant change in lithium yields would be expected for higher oxygen influxes. These results are presented in Section 5.3. From the data we find little change from both oxygen influx conditions. Although the chemical state of the surface may play a role in the decrease of lithium sputtering, uncertainty in surface coverage before, during and after bombardment of the lithium

Table 1. Correction factors of sticking coefficient for sputtered lithium atoms on a QCO crystal using VFTRIM-3D

(a) D^+ on solid deuterium saturated lithium				
E_0 (eV)	$\langle E_{Li} \rangle$ (eV)	$S^{QCM} = 1 - R_{Li}^{QCM}$	$1 + \Omega_j R_j Y_j^{QCM}$	f_c
100	5	0.833	1.001	1.201
200	8	0.820	1.002	1.221
450	10	0.807	1.004	1.244
700	30	0.808	1.004	1.243
(b) He^+ on solid deuterium saturated lithium				
E_0 (eV)	$\langle E_{Li} \rangle$ (eV)	$S^{QCM} = 1 - R_N^{QCM}$	$1 + \Omega_j R_j Y_j^{QCM}$	f_c
200	8	0.820	1.002	1.222
500	19	0.780	1.006	1.290
700	21	0.801	1.007	1.257
1000	27	0.788	1.008	1.279
(c) Li^+ on solid deuterium saturated lithium				
E_0 (eV)	$\langle E_{Li} \rangle$ (eV)	$S^{QCM} = 1 - R_N^{QCM}$	$1 + \Omega_j R_j Y_j^{QCM}$	f_c
200	11	0.800	1.000	1.250
450	17	0.788	1.003	1.273
700	22	0.783	1.003	1.281
1000	29	0.798	1.004	1.258

target leads to an error between 40 and 50%. It remains the case that with enough deuterium at the interstitial sites, preferential sputtering will dictate the effective decrease of lithium sputtering.

The next factors to consider for lithium sputtering are the magnitude of the reflected atom flux and their average energy on leaving the lithium target surface. These reflected atoms can lead to re-sputtering of deposited lithium on the QCO surface. The reflected flux from the lithium sample could reach average energies from 50 to 200 eV for incident energies of 200–700 eV for both deuterium and helium bombarding ions. This effect is lessened by deuterium atoms trapped as interstitials in the lithium BCC lattice during deuterium plasma cleaning. Deuterium embedded in lithium is shown by VFTRIM-3D calculations to decrease the incident deuterium and helium particle reflection coefficients (Fig. 2). The small fraction of high energetic neutrals is then accounted for as their probability to sputter deposited lithium on the QCM deposition crystal becomes important. However, the fraction of ions reflected as neutrals from the deuterium treated lithium surface, R_j (j for the species type), coupled to the sputtering yield of atoms from the QCM crystal surface due to these reflected neutrals, Y_j^{QCM}, and the fraction of reflected ions subtended by the QCO, Ω_j, lead to a 1–5% change in the absolute sputtering yield of lithium. Therefore, this effect can be safely neglected. In the case of lithium self-sputtering the reflection of lithium ions, R_n, is very small, according to VFTRIM-3D calculations (as shown in Fig. 5), and therefore can be safely neglected.

The calculation of the lithium sputtering yield is then possible after all of the above effects have been incorporated, with the proper uncertainty ascertained. Mass balance is then used to find an analytical expression for the absolute sputtering yield. The mass deposited on the crystal, which corresponds to the mass loss from the lithium sample due to physical sputtering, is shown to be

$$M_d = DS^{QCM} Y \Omega_{Li_2O}. \tag{1}$$

Here, D is the total ion dose, S^{QCM} is the sticking coefficient defined as $1 - R_j^{QCM}$, which corresponds to the coefficient for reflection of sputtered species j off the QCM crystal surface, Y is the absolute sputtering yield, Ω is the fraction of sputtered atoms subtended by the QCM crystal surface

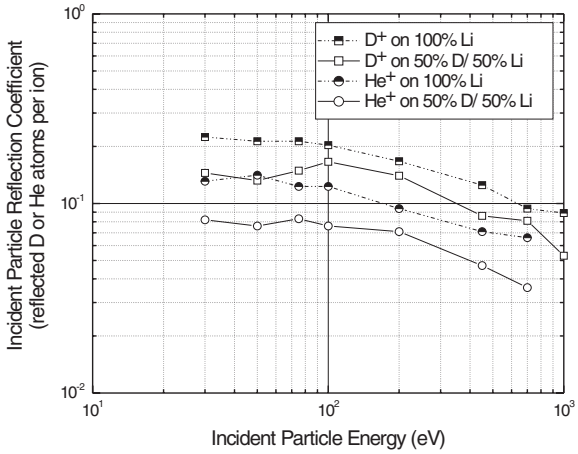

Figure 2. VFTRIM-3D computational results for the incident particle reflection coefficient of deuterium and helium incident at 45° on deuterium treated and non-deuterium-treated solid lithium.

and m_{Li_2O}, the mass of lithium oxide deposited on the QCM deposition crystal. Typical values for Ω average about 0.25–0.28. The mass deposited on the QCM crystal as measured by the XTC/2 monitor is defined as

$$M_{QCM} = \frac{\Delta f}{f_{final}} M_{crystal}. \tag{2}$$

Here Δf is the frequency change measured from the raw frequency difference between the deposition and reference crystal data corresponding to the mass collected on the QCO crystal and the mass lost due to resputtering of the deposited film from reflected incident ions, $M_{crystal}$ is the mass of the crystal given by the manufacturer and f_{final} is the final frequency after a dual QCM frequency measurement has been taken for a period between 2 and 10 h. The mass variation of the QCM is therefore defined in this manner for both low mass particle sputtering and self-sputtering,

$$M_{QCM} = \frac{\Delta f}{f} M_{crystal}. \tag{3}$$

Mass balance between the mass loss from the lithium sample and the mass gained on the QCM deposition crystal results in

Table 2. Summary of parameters used to calculate the lithium sputtering yield in the BSY model

Parameter for lithium sputtering	Deuterium	Helium	Self-sputtering
M_2/M_1	3.5	1.75	1.0
E_{th} (eV)	7.04	9.202	12.01
E_{TF} (eV)	209	557	1129
Q	0.238	0.540	0.830
f	1.212	1.215	1.217

the following expression for the lithium sputtering yield:

$$Y = \frac{1}{DS^{QCM}\Omega m_{Li_2O}} \frac{\Delta f}{f} M_{crystal}. \tag{4}$$

In alkaline metals, the fraction of sputtered particles in the ionic state can be large [22, 23]. Measurement of the dose in these experiments is done from the current collected on the lithium sample. Therefore a correction factor is needed to account for the current loss through sputtered particles in a charged state. The total ion dose to the target must compensate for the current due to secondary ion sputtering and secondary electron emission. This relationship can be written as

$$I_{Target} = I_{IN} - I^+ + I^- \tag{5}$$

where I_{Target} is the net current measured from the target, I^+ is the secondary ion current and I^- is the secondary electron emission current. With $I^- \ll I^+$ we have that the correction factor f_i for the current incident on the target is

$$f_i = \frac{I_{Target} + I^+}{I_{Target}} \tag{6}$$

so the expression for the absolute sputtering yield measured by the QCM becomes

$$Y = \frac{1}{Df_i S^{QCM}\Omega m_{Li_2O}} \frac{\Delta f}{f} M_{crystal}. \tag{7}$$

Measurement of I^+ is done by applying a negative bias to the lithium target while keeping the incident ion flux energy constant using the decelerator lens system near the target. The secondary ion yield can be measured using the QCM diagnostic by measurement of the absolute sputtering yields both of ions and neutrals and of neutrals only. These results are presented in Section 5. The difference between secondary ion fraction and secondary ion sputtering yield has been studied extensively [23].

4. Simulation and modelling

Simulations are done with the VFTRIM-3D model, which simulates surface roughness within the basic TRIM framework [15]. VFTRIM-3D includes an improved low energy binary collision model. In VFTRIM-3D the surface binding energy (SBE) provides the heat of sublimation of the material, which is a key parameter at these low energies. The version of VFTRIM-3D employed uses equipartition between the local Oen–Robinson inelastic energy loss model and the non-local Lindhard–Sharff inelastic energy loss model. Computational runs were modelled using a surface which consisted of 50 a/o lithium and 50 a/o deuterium, consistent with deuterium concentration measurements [18]. The model used a surface binding energy of 1.68 eV based on the heat of sublimation for solid lithium. The value of 1.68 eV for the surface binding energy of lithium has been measured in plasma–surface interaction experiments in PISCES-B [24]. The bond energy (BE) — the energy to break a bond in the bulk — was taken as a tenth of the SBE. Deuteration of the solid lithium surface was achieved with a deuterium plasma from a hollow cathode source with a flux of 10^{16} ions/(cm^2 s) for 20 min. This flux is sufficient to 'saturate' the surface and have enough atomic percentage of deuterium to assume a 50/50 composition at the surface over a range of at least the depth of origin of the sputtered species.

In order to complement simulation work, a widely known semi-empirical model for physical sputtering is used to study lithium sputtering. The theoretical development by Sigmund [25, 26] of physical sputtering based on a transport model has been successfully used, coupled to experimental data and appropriate scaling factors resulting in an empirical relation known as the revised Bohdansky formula [25–27], for normal incidence,

$$Y(E_0, \alpha = 0^\circ) = Qs_n^{KrC}(\varepsilon)\left[1 - \left(\frac{E_{th}}{E_0}\right)^{2/3}\right]\left(1 - \frac{E_{th}}{E_0}\right)^2. \tag{8}$$

In this case Q is known as the yield factor and is expressed as

$$Q = \frac{0.042}{U_0}\alpha(M_2/M_1) \tag{9}$$

$s_n^{KrC}(\varepsilon)$ is the nuclear stopping cross-section normalized to the reduced energy ε. The reduced energy is the ratio of E_0 and E_{TF}, where E_{TF} is the energy in the centre of mass system for a head-on collision with the screening radius as the nearest approach. The factor α is a dimensionless number dependent on the mass ratio M_2/M_1, incident energy and angle of incidence [26]. Finally, E_0 is the incident particle energy and U_0 is the surface binding energy.

The revised Bohdansky formula can be expressed as a function of the angle of incidence. A revised formula, which used the treatment by Yamamura et al. [28], results in Eq. (8) becoming

$$Y(E_0, \alpha) = Qs_n^{KrC}(\varepsilon)\left[1 - \left(\frac{E_{th}}{E_0}\right)^{2/3}\right]\left(1 - \frac{E_{th}}{E_0}\right)^2 \times \frac{1}{(\cos\alpha)^f}\exp\left[f\left(1 - \frac{1}{\cos\alpha}\right)\cos\alpha_{opt}\right]. \tag{10}$$

Values for f and α_{opt} are used as fitting parameters, while α is the incident particle angle with respect to the surface normal. A revised approach adapted by García-Rosales et al. uses an analytical fit proposed by Yamamura et al. [28] for the value of f. The empirical expression results in a weak function of f with the incident particle energy E_0 for

Table 3. Solid lithium low energy sputtering data

Incident particle energy E_0 (eV)	D^+ on D saturated lithium $Y_n \pm \Delta Y_n$	He^+ on D saturated lithium $Y_n \pm \Delta Y_n$	Li^+ on D saturated lithium $Y_n \pm \Delta Y_n$
100	0.084 ± 0.039		
200	0.138 ± 0.056	0.116 ± 0.037	0.172 ± 0.070
450	0.103 ± 0.046		0.217 ± 0.081
500		0.169 ± 0.081	
700	0.091 ± 0.033	0.154 ± 0.054	0.245 ± 0.100
1000		0.130 ± 0.048	0.158 ± 0.078

all M_2/M_1 ratios. However, experimental data [29] show that f is a strong function of the incident particle energy, E_0 for ratios less than $M_2/M_1 = 6$ down to self-sputtering values. Therefore empirical fits to these experimental data in the range of $E_0 = 100$–1000 eV are used for values of f for D, He and Li bombardment of solid lithium. Similarly, a revised approach is adapted by García-Rosales et al. for the value of α_{opt} [27]. The parameters used for semi-empirical modelling of lithium sputtering by D, He and Li bombardment are tabulated in Table 2.

In addition to the revised Bohdansky formula, an expression is used to model the saturation of the solid lithium target as a multi-component surface. In this case the expression derived by Sigmund [30] and Andersen et al. [31] based on the linear cascade theory gives the partial sputtering yield

$$Y_{Li} = Y(E_0, \alpha)\, \frac{c_{Li}}{c_D} \left(\frac{M_D}{M_{Li}}\right)^{2m} \left(\frac{U_D}{U_{Li}}\right)^{1-2m} \qquad (11)$$

where c_D is the concentration of deuterium atoms in a lithium matrix and $c_{Li} = 1 - c_D$. The U_i correspond to the surface barrier for each component. $Y(E_0, \alpha)$ is the absolute sputtering yield, as given in Eq. (10), if no component other than lithium were present on the surface. In addition, m is a parameter referring to the power potential assumed in the collision cross-section when calculating the average energy deposited in effective collisions in the lattice per incident particle [27]. The parameter m is kept fixed for all calculations with a value of a sixth for the low energy range between 100 and 1000 eV, on the basis of the existing literature [27]. The expression in Eq. (11) will be referred to as the Bohdansky–Sigmund–Yamamura (BSY) model. This expression can account for the treatment of solid lithium with deuterium atoms assuming a 50% Li–50% D surface coverage having a homogeneous composition profile. Homogeneous means that the composition is homogeneous at least over the depth of origin of the sputtered species. However, the composition profile is expected to vary with the incident ion range in lithium. Preferential sputtering, as seen in our results, is expected for the lightest component and for the least bound species [26, 32, 33].

5. Results and discussion

5.1. Energy dependence of D and He on D saturated solid Li

Figure 3 shows the experimental and computational results for D^+ on deuterium saturated lithium at 45° incidence. The chain curve represents the VFTRIM-3D simulation with open triangles, while closed triangles represent the TRIM-SP data simulating a smooth surface. The solid curve represents the calculated yield on the basis of the BSY semi-empirical model discussed in Section 4. Table 3 summarizes the data points

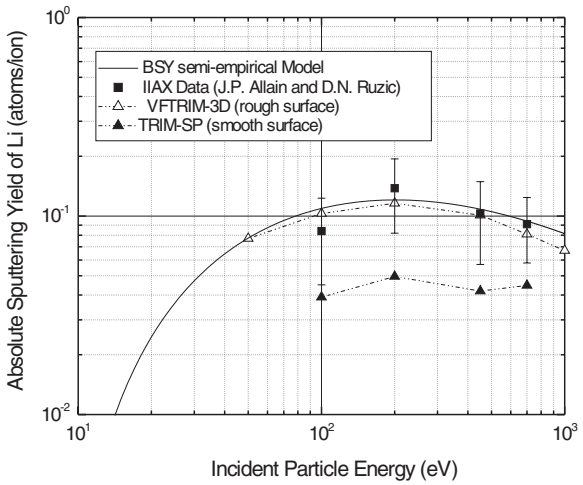

Figure 3. Experimental and computational results for the absolute lithium sputtering yield of D^+ ions incident at 45° on deuterium treated solid lithium.

with corresponding experimental errors. We can observe that the experimental and simulated yields versus incident particle energy diverge with decreasing energy primarily in the low 10–100 eV range, although the error bars are relatively large. At these lower energies the range of incoming deuterium ions extends only to a few monolayers. Over the period of the dose the surface may be enriched with more deuterium leading to a lower amount of lithium sputtered than predicted. In addition, at these lower energies, the influence of surface roughness on the sputtering yield is enhanced. This occurs due to deuterium atoms segregating to protruding regions of the surface where the net attractive force to the bulk/surface varies as r^{-3} (where r is the distance from the surface) [25] and thus the effective binding energy to the surface for these atoms drops. Studies have shown that hydrogen atoms will tend to segregate to interstitial sites in a metal lattice [34–36]. In addition, diffusion of hydrogen atoms has been measured in lithium experiments [29]. Such diffusion is not modelled by VFTRIM-3D, only that a homogeneous concentration of deuterium atoms exists in the lithium BCC lattice. Thus, the possibility for diffusion and segregation of deuterium atoms around the protruding regions of the lithium surface adds to the probability that less lithium is sputtered, since a larger amount of deuterium is preferentially sputtered. This point is also made in Fig. 3, comparing VFTRIM-3D and TRIM-SP (smooth surface) codes with the experimental data at lower energies. We expect the sputtering yield of lithium to be enhanced due to surface roughness, which is evident when comparing VFTRIM-3D and TRIM-SP data. The effect of deuterium atom diffusion/segregation on protruding regions in the rough lithium surface is demonstrated by a measured

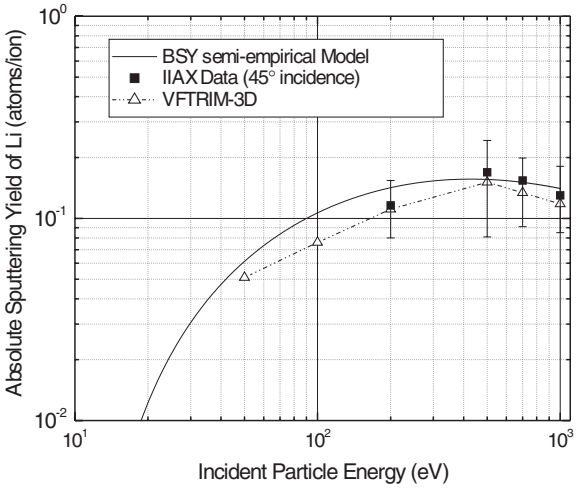

Figure 4. Experimental and computational results for the absolute lithium sputtering yield of He^+ ions incident at 45° on deuterium treated solid lithium.

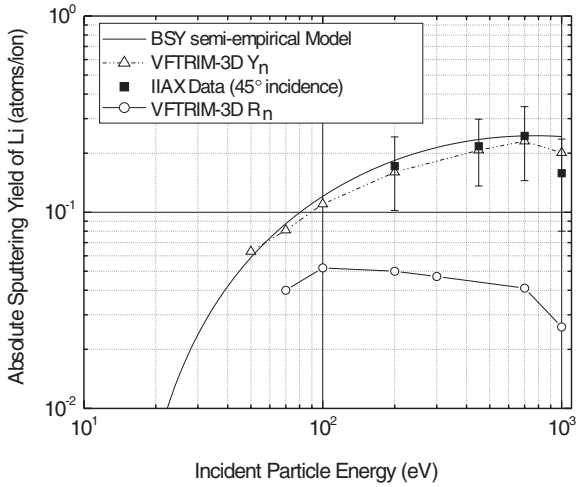

Figure 5. Experimental and computational results for the absolute lithium sputtering yield of Li^+ ions at 45° incidence on deuterium treated solid lithium. Y_n is the particle sputtering yield and R_n is the particle reflection coefficient.

reduction of lithium sputtering due to preferential sputtering of deuterium atoms, which is not accounted for by VFTRIM-3D.

At relatively higher energies than those discussed above, both the Monte Carlo VFTRIM-3D simulations and the BSY semi-empirical model predict the general functional behaviour of the yield within experimental error. The yield reaches a maximum of around 200–300 eV. The BSY model predicts an energy sputtering threshold of 15 eV, compared with 13 eV from the VFTRIM-3D simulation. At an incident particle energy of 200 eV, where the yield is a maximum, the mean sputtered energy of lithium atoms is 9.0 eV, as predicted by VFTRIM-3D.

Figure 4 shows the experimental and computational results for He^+ bombardment of deuterium treated lithium at a 45° incidence. The chain line with open triangles represents the VFTRIM-3D simulation data. The solid line represents the BSY semi-empirical model curve. The prediction made by the computational model falls within the experimental error. The functional behaviour shows the maximum of the sputtering yield of lithium at 500 eV. The BSY semi-empirical model also matches the experimental data well, except at lower energies where some of the model assumptions fail. The model predicts an energy sputtering threshold of 12 eV compared with 15 eV in the VFTRIM-3D simulation. The close match between the VFTRIM-3-D simulations and the experimental results for helium bombardment compared with deuterium and self-sputtering bombardment cases may be attributed to the fact that deuterium or lithium enrichment during sputtering does not exist. Therefore, since these mechanisms cannot be satisfactorily simulated or modelled by VFTRIM-3D or the BSY model, deviations from experimental data are expected for bombardment other than by inert species.

5.2. Lithium self-sputtering

Figure 5 shows the experimental and computational results for lithium self-sputtering at 45° incidence. Computational data using VFTRIM-3D for incident particle reflection are also included. The solid curve represents the BSY semi-empirical model curve. The experimental results are surprising. The self-sputtering yield of solid lithium is maximized at 700 eV to a value of 0.245 ± 0.100 atoms/ion. This is considerably lower than the values predicted by László and Eckstein [14]. There are two main reasons why these calculated values are significantly greater than our measured results. Firstly, the computational model employed by László and Eckstein used the TRIM-SP simulation code, which assumes a smooth surface and neglects surface roughness. Secondly, the model does not utilize a compositional component to incorporate the effect of deuterium implantation at interstitial sites of the lithium sample.

The section that follows demonstrates how important an effect this is in the sputtering of solid lithium. Within the experimental error both the simulation and semi-empirical model predict the yield functionality, except at higher energies ($E \geqslant 800$ eV) where the two begin to diverge. This is due to the shorter mean range of the incident lithium ions in solid lithium compared with those of deuterium or helium. Thus, a large percentage of the lithium ion kinetic energy is distributed among the top-most surface deuterium atoms, which leads to a preferentially larger deuterium erosion and a reduction of lithium sputtering.

5.3. Dependence on deuterium treatment and oxygen coverage of lithium surface

The dependence of lithium surface deuterium treatment plays a significant role in the absolute sputtering yield of solid lithium. Figure 6 shows experimental and VFTRIM-3D simulation results for He^+ bombardment on deuterium treated and non-deuterium-treated lithium at 45° incidence. Two sets of data for the non-deuterium-treated case are shown. One for an incident background oxygen flux of the order 10^{10} atoms/(cm^2 s), the other for 10^{13} atoms/(cm^2 s). The energy dependence of the absolute sputtering yield of lithium in atoms per incident ion is plotted in Fig. 6. The lithium sputtering yield functional behaviour of the non-deuterium-treated lithium target is shifted towards a maximum at higher energies (∼1000 eV) for one

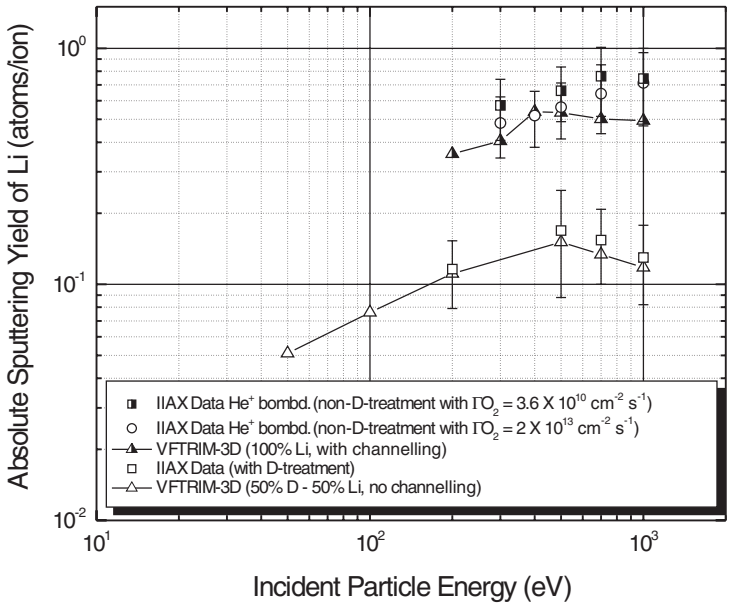

Figure 6. Energy dependence of 45° incidence He^+ bombardment on non-deuterium-treated and deuterium treated solid lithium measurements and the VFTRIM-3D simulation.

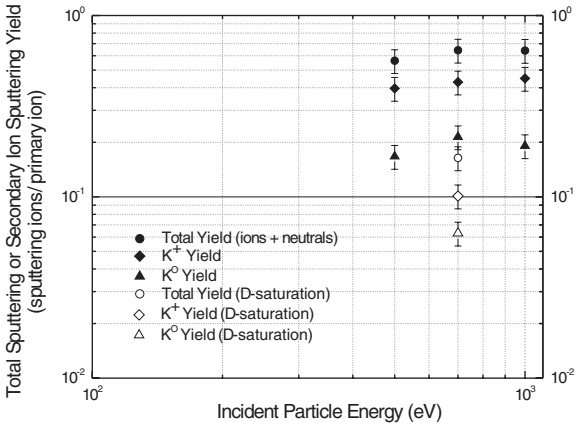

Figure 7. Energy dependence of secondary Li^+ sputtering yield of He^+ bombardment on non-deuterium-saturated and deuterium saturated solid lithium at 45° incidence. K^+ is the secondary ion sputtering yield and K^0 is the neutral sputtering yield.

of the experimental cases. The VFTRIM-3D results begin to diverge from the experimental data at energies above 500 eV. In addition, the computational model used for the non-deuterium-treated data is based on a mechanism for channelling energy from subsurface layers to the top layer [7]. The simulation model used to predict the deuterium treated data does not utilize this mechanism. This result implies that the absence of deuterium atoms at interstitial sites of the lithium BCC lattice allows for atoms from deeper in the sputtering cascade to transfer their momentum up to surface layer atoms, thus contributing to more sputtering.

The deuterium treated lithium sputtering yield is measured to be significantly lower than that for bombardment with no deuterium treatment. The chemical state of the lithium surface is relevant since the incident oxygen flux on the surface is similar to the incident ion flux. However, this factor is only minor when comparing the two sets of experimental data in Fig. 6. The lithium sputtering yield changes very little within the experimental error when the incident oxygen flux varies by three orders of magnitude. The main factor that dominates this result, therefore, is preferential sputtering of deuterium atoms. As explained in Section 4, preferential sputtering is expected for the lightest component and for the least bound species. The deuterium is sputtered preferentially and the surface, in time, is enriched in lithium. However, at our doses and doses found in typical plasma facing conditions in tokamaks, the one to one ratio of lithium matrix atoms and saturating deuteride species is kept over the depth of origin of sputtered species as a constant flux of deuterium atoms impinges on the lithium sample and a source of implanted deuterium atoms segregates to the surface over the time of the dose [37–39]. Another factor is the competition between preferential sputtering on the one hand, and mixing or segregation on the other [40, 41]. These latter effects are less pronounced here since we have a surface that is 'soaked' with deuterium atoms and not an alloy composed of deuterium and lithium constituents. Therefore preferential sputtering mechanisms are justified as a viable interpretation. Binding of deuterium and lithium atoms is less likely than deuterium atoms penetrating BCC lithium and occupying interstitial sites.

5.4. Energy dependence of secondary ion sputtering yield and secondary ion fraction

The energy dependence of the secondary ion sputtering yield for He^+ bombardment on deuterium treated and non-deuterium-treated lithium is shown in Fig. 7. This measurement is important since, in a fusion device, plasma sputtered ions will immediately return to the surface due to the sheath potential, and thus not contribute to the sputtering yield [33]. The ion yield does not vary significantly in the range 500–1000 eV. The fraction of sputtered atoms in the ionic state is measured to be about 65% or two out of three sputtered atoms leave as ions. The results for deuterium surface treatment on

the ion yield shows that the total number of lithium atoms sputtered is decreased as discussed in Section 5.3. Therefore, in terms of ion yield, the total yield consequently decreases with deuterium saturation. These results are consistent with the measured values of ion yields from other alkaline metals [42].

6. Conclusions

The lithium sputtering yields for D^+, He^+ and Li^+ bombardment of lithium in the solid phase have been measured. The self-sputtering yield of lithium is found to be considerably lower than that predicted by earlier simulations [14]. This is primarily due to the influence of deuterium treatment of the lithium surface and deuterium preferential sputtering during bombardment. VFTRIM-3D is able to predict the IIAX experimental data within experimental error for most data. Our results lead to the conclusion that deuterium atoms will diffuse to interstitial locations within the BCC lithium lattice leading to preferential sputtering, and thus decrease the absolute sputtering yield of lithium. In addition to VFTRIM-3D simulations, the BSY semi-empirical model has been used to demonstrate the functionality of the lithium sputtering yield and its relation to experimental data. Although we assert that deuterium plays a major role in lithium sputtering, the chemical state of the surface prior to ion bombardment is also important.

In addition to preferential sputtering, the fraction of sputtered atoms in the ionic state has been measured in IIAX and reaches close to 65% for Li, D and He bombardment. This means that the yield of lithium neutrals is about a third the lithium sputtering yields presented. The sputtering lithium yield from bombardment by D, He and Li ions is found to be well below unity, strengthening the viability of lithium as a future plasma facing material.

Acknowledgements

This work is supported by the US Department of Energy (DOE) ALPS Program and the US DOE/NSF Basic Plasma Science Initiative (No. DE-FG02-97ER54440). We would like to thank M. Hendricks, R. Ranjan, M. Boaz, M. Lazebnik and L. Manohar for their support in assisting with measurements and analysis. We are also grateful to N. Finnegan and R. Haasch for their help with AES and XPS measurements carried out in the Center for Microanalysis of Materials, University of Illinois, which is supported by the US DOE under Grant No. DEFG02-96-ER45439. In addition, we would like to thank J. Brooks and P. Sigmund for helpful and insightful discussions.

References

[1] Atomic and Plasma–Material Interaction Data for Fusion 1991 *Nucl. Fusion* (Suppl.) vol 1 (Vienna: IAEA)
[2] Post D.E. and Behrisch R. (eds) 1984 *Physics of Plasma–Wall Interactions in Controlled Fusion (NATO ASI Series, Series B: Physics)* vol 131 (New York: Plenum) p 99
[3] Gauster W.B. and Spears W.R. 1994 *Atomic and Plasma–Material Interaction Data for Fusion (Suppl. to Nucl. Fusion)* vol 5 (Vienna: IAEA) p 7
[4] Gauthier E., Eckstein W., László J. and Roth J. 1990 *J. Nucl Mater.* **176, 177** 438
[5] Roth J. 1999 *J. Nucl. Mater.* **266–269** (1999) 51
[6] Davis J.W. and Haasz A.A. 1997 *J. Nucl. Mater.* **241–243** 37
[7] Smith P.C. and Ruzic D.N. 1998 *Nucl. Fusion* **38** 683
[8] Thomas P.R. and JET Team 1990 *J. Nucl. Mater.* **176, 177** 3
[9] Roth J. 1990 *J. Nucl. Mater.* **176, 177** 132
[10] Roth J., Eckstein W. and Bohdansky J. 1989 *J. Nucl. Mater.* **165** 199
[11] Kato S., Watanabe M., Toyoda H. and Sugai H. 1999 *J. Nucl. Mater.* **266–269** 406
[12] Ruzic D.N., Monica M.C., Allain J.P. and Budny R.V. 1999 *J. Nucl. Mater.* **266–269** 1303
[13] Brooks J. *et al* 2001 *J. Nucl. Mater.* **290–293** 185
[14] László J. and Eckstein W. 1991 *J. Nucl. Mater.* **184** 22
[15] Ruzic D.N. 1990 *Nucl. Instrum. Methods* B **47** 118
[16] Smith P.C. and Ruzic D.N. 1999 *J. Vac. Sci. Technol.* **17** 3443
[17] Zalm P.C. 1989 *Handbook of Ion Beam Processing Technology* ed J.J. Cuomo, S.M. Rossnagel and H.R. Kaufman (Park Ridge, NJ: Noyes Publications) p 78
[18] Sugai H. 1996 *Vacuum* **47** 981
[19] Pulker H.K. and Decosterd J.P. 1984 *Applications of Piezoelectric Quartz Crystal Microbalances* ed C. Lu and A.W. Czanderna (Amsterdam: Elsevier)
[20] Márquez A., Vargas A. and Balbuena P. 1998 *J. Electrochem. Soc.* **145** 33
[21] Solin S.A. and Zabel H. 1988 *Adv. Phys.* **37** 87
[22] Kraus A.R. and Gruen D.M. 1979 *J. Nucl. Mater.* **85, 86** 1179
[23] Blaise G. 1978 *Material Characterization using Ion Beams* ed J.P. Thomas and A. Cachard (New York: Plenum)
[24] Doerner R.P. *et al* 2001 *J. Nucl. Mater.* **290–293** 166
[25] Sigmund P. 1969 *Phys. Rev.* **184** 383
[26] Sigmund P. 1969 *Phys. Rev.* **187** 768
[27] García-Rosales C., Eckstein W. and Roth J. 1994 *J. Nucl. Mater.* **218** 8
[28] Yamamura Y. Itikawa Y. and Itoh N. 1983 *Angular Dependence of Sputtering Yields of Monatomic Solids, Report IPPJ-AM-25* Institute of Plasma Physics, Nagoya
[29] Eckstein W., García-Rosales C., Roth J. and Ottenberger W. 1993 *Sputtering Data* Max-Planck-Institut für Plasmaphysik, Garching
[30] Sigmund P. 1981 Sputtering by particle bombardment I *Topics in Applied Physics* vol 47, ed R. Behrisch (Berlin: Springer)
[31] Andersen N. and Sigmund P. 1974 *Mat. Fys. Medd. Dan. Vid. Selsk* **39** 1
[32] Stepanova M.G. 1995 *Phys. Chem. Mech. Surf.* **10** 1179
[33] Sigmund P. 1980 *J. Vac. Sci. Technol.* **17** 396
[34] Myers S.M., Richards P.M. and Wampler W.R. 1989 *J. Nucl. Mater.* **165** 9
[35] Wampler W.R. 1984 *J. Nucl. Mater.* **122, 123** 1598
[36] Haasz A.A. and Davis J.W. 1997 *J. Nucl. Mater.* **241–243** 1076
[37] Sigmund P. 1987 *Nucl. Instrum. Methods* B **27** 1
[38] Falcone G. and Sigmund P. 1981 *Appl. Phys.* **25** 307
[39] Sigmund P. 1993 *Mat. Fys. Medd. Dan. Vid. Selsk.* **43** 255
[40] Sigmund P. and Oliva A. 1993 *Nucl. Instrum. Methods* B **82** 269
[41] Sigmund P. and Glazov L.G. 2000 *Nucl. Instrum. Methods* B **164, 165** 453
[42] Navinsek B. 1965 *J. Appl. Phys.* **36** 1678